15th World Congress on Computational Mechanics (WCCM-XV)
8th Asian Pacific Congress on Computational Mechanics (APCOM-VIII)
Virtual Congress: 31 July – 5 August 2022
S. Koshizuka (Ed.)

A DISCRETE EXTERIOR CALCULUS BASED FRAMEWORK FOR CFD

PANKAJ JAGAD[*1], BHARGAV MANTRAVADI[*2], MINMIAO WANG[*3], ABDULLAH ABUKHWEJAH[*4] AND RAVI SAMTANEY[*5]

[*] King Abdullah University of Science and Technology
Thuwal, Saudi Arabia
[1] pankaj.jagad@kaust.edu.sa
[2] bhargav.mantravadi@kaust.edu.sa
[3] minmiao.wang@kaust.edu.sa
[4] abdullah.abukhwejah@kaust.edu.sa
[5] ravi.samtaney@kaust.edu.sa

Key words: Discrete exterior calculus, vortex dynamics, multiphase flows, flows on surfaces.

Abstract. *We present a framework for computing flows on surfaces based on a discrete exterior calculus (DEC) discretization of Navier-Stokes (N-S) equations on simplicial meshes. The framework incorporates primitive formulation of the N-S equations and allows for a time integration method which features energy conservation [1]. Other features of the framework consist of the inclusion of the Coriolis force term to investigate flows on rotating surfaces, and an interface tracking method for multiphase flows. The method is second order accurate on structured triangular meshes, and first order on otherwise unstructured meshes, and demonstrates the conservation of inviscid invariants such as kinetic energy and enstrophy over an extended period of time [2].*

1 INTRODUCTION

Exterior calculus is a generalization of vector calculus to manifolds of arbitrary dimension. DEC [3] is the discrete version of exterior calculus. In DEC, physical fields are discretely expressed as k-forms representing the integration of the physical quantity on k-dimensional primal/dual mesh objects. DEC ensures that vector calculus identities are discretely satisfied. In addition to preserving the mathematical properties it allows for conservation of secondary quantities, such as kinetic energy and vorticity for an inviscid flow [4, 2]. DEC is coordinate independent, and convenient for investigating flows over curved surfaces. We develop a DEC discretization method for incompressible flow Navier-Stokes equations. We present simulation results for a variety of physical configurations including the flow past a circular cylinder [5] and airfoils, multiphase flow of immiscible incompressible fluids [6], and vortex dominated flows on surfaces with and without rotation [7].

2 NUMERICAL METHOD

The N-S equations for an incompressible flow of a single-phase fluid with constant properties on a smooth Riemannian surface, in a rotating frame of reference, read

$$\frac{\partial \mathbf{v}}{\partial t} - \mu \left[-\Delta^{dR}\mathbf{v} + 2\kappa\mathbf{v} \right] + \nabla_{\mathbf{v}}\mathbf{v} + \mathrm{grad}_S p + f\hat{k} \times \mathbf{v} = 0, \tag{1}$$

$$\mathrm{div}_S \mathbf{v} = 0, \tag{2}$$

where $\mathbf{v}$ is the tangential surface velocity, p is the effective surface pressure including the centrifugal force, μ is the dynamic viscosity, Δ^{dR} is the surface Laplace-DeRham operator, κ is the surface Gaussian curvature, $\nabla_{\mathbf{v}}$ is the covariant directional derivative, grad_S is the surface gradient, div_S is the surface divergence, f is the Coriolis parameter, and $\hat{k}$ is the unit vector in the direction of the axis of rotation. We discretize these equations with a DEC method. The discretized equations read

$$\left[\left(-\tfrac{1}{\Delta t}+\mu k\right) I + \tfrac{1}{2}\mu \mathrm{d}_0 *_0^{-1} \left[-\mathrm{d}_0^T\right] *_1 - \tfrac{1}{2}\left(W_V\right)^{n+1} *_0^{-1} \left[-\mathrm{d}_0^T\right] *_1\right] \left(U^*\right)^{n+1} + *_1^{-1} \mathrm{d}_1^T \left(P^d\right)^{n+\frac{1}{2}} = F, \tag{3}$$

$$\begin{aligned} F = {} & \left(-\tfrac{1}{\Delta t}-\mu k\right)\left(U^*\right)^n - \tfrac{1}{2}\mu \mathrm{d}_0 *_0^{-1} \left(\left[-\mathrm{d}_0^T\right] *_1 \left(U^*\right)^n + \mathrm{d}_b\left(V\right)^n + \mathrm{d}_b\left(V\right)^{n+1}\right) + \tfrac{1}{2}\left(W_V\right)^{n+1} *_0^{-1} \mathrm{d}_b\left(V\right)^{n+1} \\ & + \tfrac{1}{2}\left(W_V\right)^n *_0^{-1} \left(\left[-\mathrm{d}_0^T\right] *_1 \left(U^*\right)^n + \mathrm{d}_b\left(V\right)^n\right) + \tfrac{1}{2}\left[\left(W_V\right)^{n+1} + \left(W_V\right)^n\right] *_0^{-1} f_{dual2}, \end{aligned} \tag{4}$$

$$\left[d_1\right]\left(U^*\right)^{n+1} + \left[0\right]\left(P^d\right)^{n+\frac{1}{2}} = 0. \tag{5}$$

The details of discretization, and the definition and expressions of the discrete operators are available in [2]. The set of non-linear equations (3) - (5) is solved using Picard's iterative method for the mass flux 1-form $\left(U^*\right)$ and dynamic pressure $\left(P^d\right)$ degrees of freedom. We verify/validate the method, and evaluate the convergence of the L^2-norm of the velocity one-form (flux) and the interpolated velocity vector errors with mesh size as well as that of the kinetic energy relative error, which is reported in Ref. [2].

3 RESULTS AND DISCUSSION

3.1 Flow past a cylinder on curved surfaces

We investigate the dynamics of flows past a stationary circular cylinder embedded on spherical and cylindrical surfaces at Reynolds numbers (based on the cylinder diameter D) $Re = 40, 100$, and 1000. We vary the normalized embedding surface curvature values κD, where κ is the maximum principal curvature, from 0 (flat surface) to 1/12. We compute the parameters of dynamical importance such as the drag coefficient, the lift coefficient and Strouhal number and compare them with that for the flow past a cylinder embedded on a flat surface of an equivalent domain size and the same boundary conditions. For the range of parameters considered, the effect of the embedding surface curvature is found to be insignificant. Figure 1 shows a representative snapshot of vortex streets.

3.2 Flow past an airfoil

We investigate the dynamics of flow past NACA0012 airfoil at different angles of attack (α), and at Reynolds number, based on the chord length, $Re = 1000$. A comparison of the mean pressure coefficient, that of the mean drag coefficient, and that of the mean lift coefficient with that published in the literature shows a good agreement. Figure 2 shows the vortex patterns.

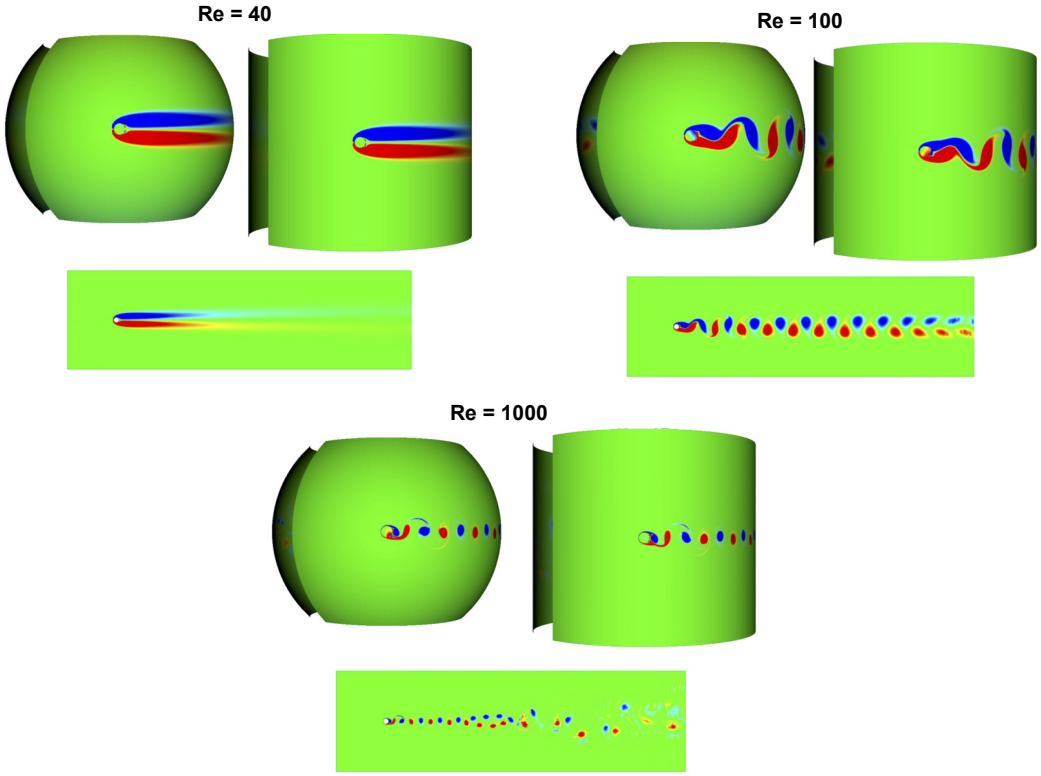

Figure 1: Vortex streets for flow past a cylinder at Reynolds number Re = 40, 100, and 1000. The radius of the embedding spherical and cylindrical surfaces R = 12. The classical flat surface case is included for comparison. The effect of the embedding surface curvature on the flow dynamics is insignificant.

3.3 Flow past a cylinder with a bump in the wake

Figure 3 shows the vortex street for the flow past a stationary circular cylinder with a Gaussian bump in the wake at $Re = 100$. The bump is described by

$$z = h\exp\left(-\left((x-x_0)^2+(y-y_0)^2\right)/\left(2r_0^2\right)\right), \tag{6}$$

where the parameters describing the bump location are $x_0 = 6.0, y_0 = 0, h = 1.6, 1/\left(2r_0^2\right) = 0.4$. Here, x, y, and z are the streamwise, cross-stream and spanwise directions, respectively. Although the Gaussian curvature generates vorticity, the vorticity in the wake dominates.

3.4 Vortex dynamics on a non-rotating sphere

Figure 4 shows evolution of vortical structures on a non-rotating unit sphere from a random initial distribution of point vortices for the viscosity $\mu = 10^{-3}$ and $\mu = 10^{-5}$. Initially, 200 vortices are considered. The initial vorticity distribution is expressed as $\omega = \Gamma/\cosh^2(3r/a)$, where Γ, a, and r are the vortex strength, the vortex radius and the distance between any field point and the vortex center. A constant strength $\Gamma = \pm 3$ is chosen for all vortices. The vortex radius $a = 0.075$ is chosen. As the solution evolves, the like-signed vortices merge together to form large scale structures. At late times, a dipolar or quadrupolar vortical structure is formed for $\mu = 10^{-3}$ and $\mu = 10^{-5}$, respectively.

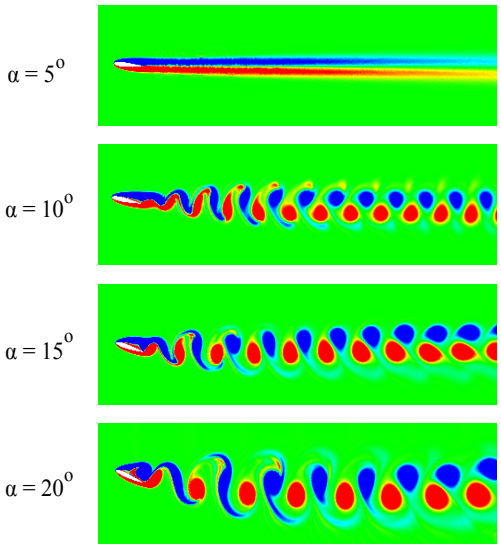

Figure 2: Vortex patterns for flow past NACA0012 at different α and $Re = 1000$.

3.5 Harmonic waves on a rotating sphere

The stationary solution for the motion of harmonic waves on a rotating sphere (usually used as a model to the Rossby waves in the earth's atmosphere) is [8]

$$\psi(\phi,\theta) = A\sin m\phi P_l^m(\cos\theta) - BR^2\cos\theta, \tag{7}$$

where, ψ is the stream function, ϕ is longitude, θ is colatitude, A is an arbitrary constant, $B = \frac{2\Omega}{l(l+1)-2}$, P_l^m is associated Legendre polynomial of degree l and order m, R is sphere radius, and Ω is the rate of rotation of the sphere. The viscosity is assumed to be zero. Figure 5 shows no distortion of the stream function (ψ) distribution, and the stationary state is preserved even after a simulation time of 21 days.

3.6 Rayleigh-Taylor instability

We extend the DEC method to two-phase flows by including volume of fluid and phase-field [6] equations. Here, we investigate Rayleigh-Taylor instability (RTI) at Atwood number $At = (\rho_h - \rho_l)/(\rho_h + \rho_l) = 0.05,\ 0.1,$ and 0.5 using the volume of fluid formulation. Here, ρ_h and ρ_l are the densities of the heavier fluid and the lighter fluid, respectively. Unit viscosity ratio is assumed with $\mu = 0.0001$ for each fluid. The interface between the lighter (at the bottom) and the heavier fluids (at the top) is perturbed initially as $\eta = \eta_0\cos\left(\frac{2\pi x}{L} - \pi\right)$, where $\eta_0 = 0.02$, and $L = 2$. The theoretical linear growth rate of the interface (for inviscid flow) is computed as $\gamma = \sqrt{Atgk} = 1.211,\ 1.756,$ and 3.925 for $At = 0.05,\ 0.1$ and 0.5, respectively. Here, g is the gravitational acceleration and $k = 2\pi/\lambda$ is the wavenumber with λ standing for the wavelength. Figure 6 shows the growth rate of the kinetic energy (KE) for the simulations. Numerically, the interface growth rate $\gamma = m/2$, where m is the KE growth rate. The comparison of the linear growth rate with the theoretical one shows a good agreement.

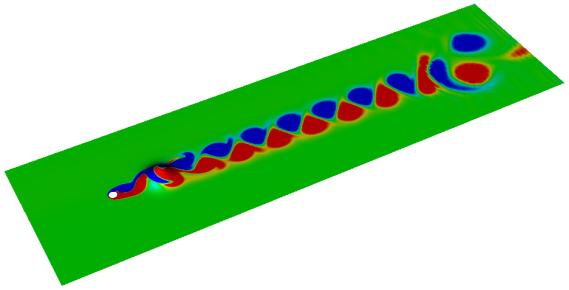

Figure 3: Vortex streets for flow past a cylinder with a Gaussian bump in the wake at $Re = 100$. There is insignificant effect of the vorticity generated by the Gaussian bump on the flow dynamics.

4 CONCLUSIONS

We present a DEC based scheme for discretization of incompressible N-S equations for flows on curved surfaces. We present various cases of flows on surfaces with and without rotation. The method exhibits second and first order relative error convergence rate (for the velocity 1-form) with the mesh size for the structured triangular meshes and the otherwise unstructured meshes, respectively. There is second order kinetic energy relative error convergence with the mesh size. The dynamics of flow past a cylinder embedded on a curved surface is independent of the curvature of the embedding surface for the set of parameters considered here. The vorticity generated by the cylinder wake dominates over that generated by the presence of a Gaussian bump in the wake. There is dipolar or quadrupolar vortical state at late times for the evolution of vorticity from an initial distribution of point vortices on a non-rotating sphere. The method preserves the initial stationary state for a rotating sphere for an extended period of time. We extend the method to two-phase immiscible incompressible flows. The linear growth rate of the interface for RTI is in good agreement with the theoretical one.

REFERENCES

[1] P. Mullen, K. Crane, D. Pavlov, Y. Tong, and M. Desbrun. Energy-preserving integrators for fluid animation. *ACM Trans. Graph.*, 28(3):38, 2009.

[2] Pankaj Jagad, Abdullah Abukhwejah, Mamdouh Mohamed, and Ravi Samtaney. A primitive variable discrete exterior calculus discretization of incompressible Navier-Stokes equations over surface simplicial meshes. *Physics of Fluids*, 33(1):017114, 2021.

[3] A. N. Hirani. *Discrete exterior calculus*. PhD thesis, California Institute of Technology, 2003.

[4] M. S. Mohamed, A. N. Hirani, and R. Samtaney. Discrete exterior calculus discretization of incompressible Navier-Stokes equations over surface simplicial meshes. *Journal of Computational*

Physics, 312:175–191, 2016.

[5] Pankaj Jagad, Mamdouh S Mohamed, and Ravi Samtaney. Investigation of flow past a cylinder embedded on curved and flat surfaces. *Physical Review Fluids*, 5(4):044701, 2020.

[6] Minmiao Wang, Pankaj Jagad, Anil N Hirani, and Ravi Samtaney. Discrete exterior calculus discretization of two-phase incompressible Navier-Stokes equations with a conservative phase field method. *arXiv preprint arXiv:2203.13070*, 2022.

[7] Pankaj Jagad and Ravi Samtaney. Effects of rotation on vorticity dynamics on a sphere with discrete exterior calculus. *Physics of Fluids*, 33(10):107117, 2021.

[8] SM Neamtan. The motion of harmonic waves in the atmosphere. *Journal of Meteorology*, 3(2):53–56, 1946.

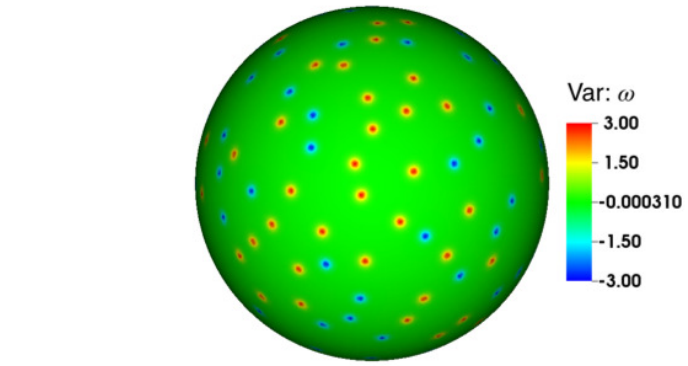

(a)

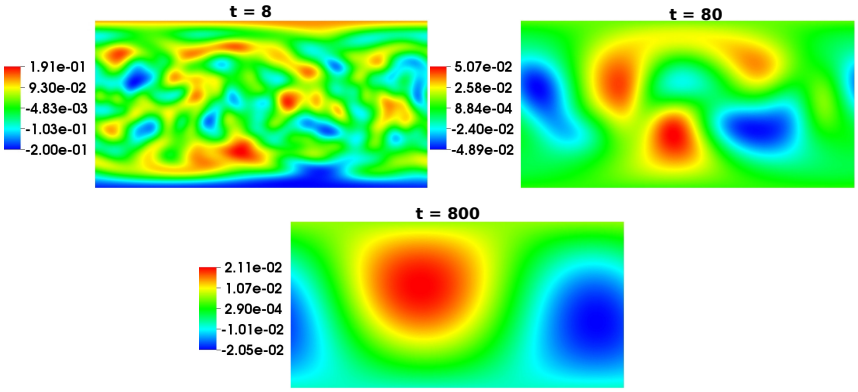

(b)

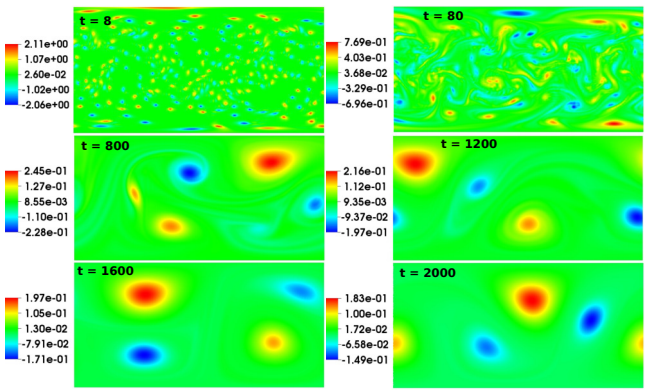

(c)

Figure 4: Evolution of vortical structures on a non-rotating sphere from a random initial distribution of point vortices. (a) initial condition, (b) $\mu = 10^{-3}$: leads to dipolar vortical structure at late times, (c) $\mu = 10^{-5}$: leading to a quadrupolar vortical structure at late times.

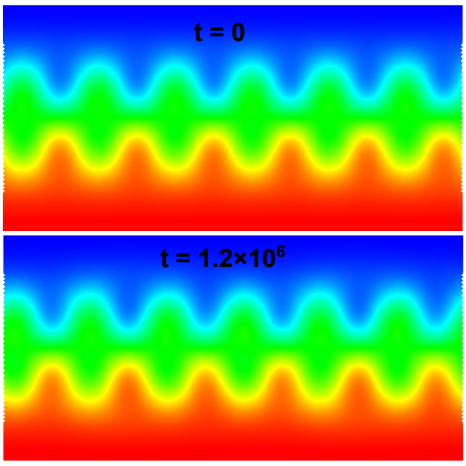

Figure 5: Stream function distribution showing that the stationary state is preserved for the motion of harmonic waves on a rotating sphere

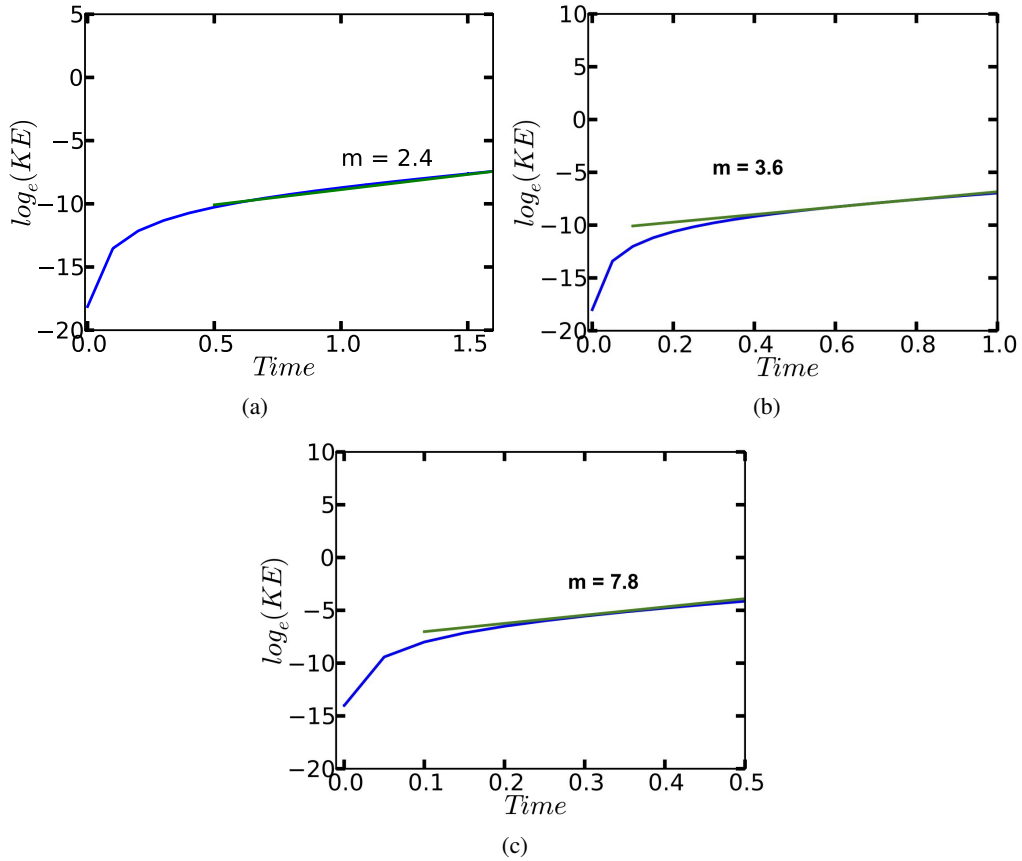

Figure 6: Kinetic energy growth rate for the Rayleigh-Taylor instability case. (a) $At = 0.05$, (b) $At = 0.1$, (c) $At = 0.5$